AGU ADVANCING EARTH AND SPACE SCIENCES

Geophysical Research Letters

RESEARCH LETTER
10.1029/2024GL112957

Stratigraphic Evidence of Backwater Morphodynamics and Lowland River Deltas in the Northern Hemisphere of Mars

C. M. Hughes[1], **J. B. Shaw**[1], **A. M. Fernandes**[2], **and T. E. Swanson**[3]

[1]Department of Geosciences, University of Arkansas, Fayetteville, AR, USA, [2]Department of Earth and Environmental Sciences, Denison University, Granville, OH, USA, [3]The Water Institute, Baton Rouge, LA, USA

Key Points:

- Martian river delta channel belts exhibit characteristic narrowing associated with backwater morphodynamics as on Earth
- Results indicate that backwater morphodynamics are expected to be present on all planetary bodies with fluvial-deltaic systems
- Deposits in Mars' northern hemisphere are similar to large, long-lived, lowland river deltas on Earth

Correspondence to:

C. M. Hughes,
ch117@uark.edu

Citation:

Hughes, C. M., Shaw, J. B., Fernandes, A. M., & Swanson, T. E. (2025). Stratigraphic evidence of backwater morphodynamics and lowland river deltas in the Northern Hemisphere of Mars. *Geophysical Research Letters*, *52*, e2024GL112957. https://doi.org/10.1029/2024GL112957

Received 9 OCT 2024
Accepted 28 MAY 2025

Abstract

Backwater morphodynamics describe feedbacks between hydraulics and sedimentation in fluvio-deltaic systems in the coastal backwater zone. On Earth, normalized channel belt width decreases approaching the coastline and drops sharply at the start of the backwater zone. This systematic decrease allows a *backwater/belt-width window* to be defined, one backwater length upstream from the coast with normalized widths from 2 to 6. We use the *backwater/belt-width window* to interpret backwater morphodynamics and estimate backwater length on Mars using narrowing channel belts at Aeolis Dorsa. We measure nine belts from martian delta deposits and compare normalized width to distance upstream from an ancient shoreline. Estimates range from ∼5 to 17 km, coinciding with lengths derived from avulsions. Observing these relationships on Mars demonstrates the universality of backwater morphodynamics, providing new methods for understanding martian hydrologic history. Notably, our results indicate Aeolis Dorsa deltas resembled lowland river deltas on Earth, consistent with a northern hemispheric ocean.

Plain Language Summary

This study explores how specific hydraulic and sedimentation patterns, referred to as backwater morphodynamics, occur in river systems near the coast, and whether these patterns also exist on Mars. On Earth, we observe, in river systems like the Mississippi, the width of the channel belt (the region where a river distributes sand) decreases to roughly 2–6 times the channel width within what we call the *backwater/belt-width window*. We measured the widths of nine river delta channel belts from the surface of Mars and found their *backwater/belt-width window* upstream from an ancient shoreline. The locations of these windows provide an estimate for the length scale of the backwater zone for each delta, which notably coincides with the location of avulsion nodes. The confirmation of these relationships in martian stratigraphy demonstrates that backwater morphodynamics is a planetary phenomenon and should be present on all planets with river systems, whether ancient or active (e.g., Earth, Mars, and Titan). Backwater morphodynamic relationships can be used as a tool to discover other important characteristics about river systems, like paleogeography, slope, and grainsize. Importantly, our results provide new evidence consistent with an ancient ocean in the northern hemisphere of Mars.

1. Introduction

Reconstructing Mars' hydrologic and fluvial history is essential for understanding the climatic history and the past habitability of the Red Planet. Decades of research indicate Mars experienced periods of sustained global hydrologic activity, including evidence pointing to the possibility of a northern hemispheric ocean (e.g., Li et al., 2025). Despite these advancements, the exact nature of Mars' ancient climate, habitability, and the possibility of an ocean remains underdetermined.

Many published studies describe quantitative analyses of martian fluvial deposits, but few have directly leveraged coastal hydrodynamic principles such as backwater morphodynamics. Backwater morphodynamics describe the interplay between changing fluid dynamics and sedimentation in rivers near coastlines. By focusing on the backwater characteristics of coastal deposits on Mars, we extract robust estimates for paleo-slope, grain size, and interpretations of avulsion dynamics and paleogeography. Our results point to long-lived lowland river deltas north of the hemispheric dichotomy, unbounded by crater topography and therefore consistent with that of a northern ocean or sea.

1.1. Backwater Morphodynamics

Backwater morphodynamics exist where a river responds hydrodynamically to the standing body of water at its terminus with a transition from a uniform flow (spatially invariant flow velocities) to non-uniform flow (spatially variant flow velocities; Te Chow, 1959). The backwater length scale, L_b, is the distance upstream from the coastline to the start of the backwater zone and it may be estimated by

$$L_b = \frac{h}{s} \tag{1}$$

where h is a characteristic channel depth and s is a characteristic slope (Paola & Mohrig, 1996). Geometrically, the start of backwater zone is where the average channel bed elevation drops below sea level.

Numerous hydro-geomorphic changes occur in the backwater zone. For example, in backwater-modulated rivers, rates of lateral channel migration increase and then decrease near the coast (Hudson & Kesel, 2000; Lamb et al., 2012; Smith et al., 2020; Wu et al., 2023). During low discharge at the start of the backwater zone, flow decelerates, and channels deepen, resulting in aggradation and diminished bedload transport downstream. During floods, steepened water surface slopes increase bedload and cause erosion near the channel mouth (e.g., Nittrourer et al., 2012). In association with aggradation at the start of the backwater zone, several studies have linked the length of lobe-scale avulsions to the L_b in lowland river deltas (e.g., Brooke et al., 2020; Chatanantavet et al., 2012; Ganti et al., 2016; Jerolmack & Swenson, 2007; Shaw & McElroy, 2016).

1.2. Backwater Morphodynamics in the Rock Record

Fernandes et al. (2016) show evidence of backwater morphodynamics in stratigraphy with a decrease in the normalized channel belt width of the Mississippi, Waal, Nederrijn-Lek, and Linge rivers near their coastlines (channel belts referred to as CBs throughout the text; considered equivalent to channel bodies, as defined by Gibling, 2006). Normalized CB width refers to the non-dimensional quantity calculated by dividing measured CB width by the characteristic channel width. Notably, at approximately one L_b upstream from the coastline, normalized CB widths converge and decrease precipitously toward a value of 1 in the direction of the coast (Figure 1a). We define this convergence at ∼one L_b as the *backwater/belt-width window* (pink box in Figure 1a). Downstream of this point, channel belt width decreases to the channel width, and upstream the channel-normalized width remains large. Wahbi and Blum (2023) document similar behavior in the Paraná, Niger, Indus, and Irrawaddy deltas. Martin et al. (2018) and Wu et al. (2023) recognize similar trends in the Triassic delta deposits of the Mungaroo Formation off the coast of Australia and the Devonian delta deposits of the Tullig Sandstone of Ireland respectively.

1.3. Backwater Morphodynamics on Mars

River delta deposits have been identified on Mars in the southeast Aeolis Dorsa region (DiBiase et al., 2013; Hughes et al., 2019; approx. coordinates: −6.192°, 154.289). These deposits are topographically inverted and appear as narrow, quasi-sinuous ridges and plateaus. Topographic inversion takes place when coarse-grained channel sediment is less erodible than the fine-grained floodplain material. On Mars, aeolian processes preferentially erode floodplain deposits leaving "fluvial ridges" behind (e.g., Pain et al., 2007).

Given the deltas on Mars, it stands that backwater morphodynamics influenced martian sedimentation. Prior studies have identified potential evidence of backwater effects, but few have tested this systematically. Fawdon et al. (2018) interpret divergent lineations on the Hypanis Vallis fan system as backwater-modulated avulsions. Cardenas et al. (2018) interpret valley-fills in southeast Aeolis Dorsa as evidence for a dynamic base-level and backwater influence, although Ahmed et al. (2023) later conclude that these deposits do not record backwater effects. Ahmed et al. (2023) estimate L_b of the deposits in southeast Aeolis Dorsa to be ∼3.66 km by combining estimates of channel width, depth, and slope with the models proposed by Lapôtre et al. (2019). Goudge et al. (2018) study the Jezero crater west-fan and provide an order of magnitude estimate for L_b (a few hundred meters to a few kilometers). DiBiase et al. (2013) use avulsion length as a proxy for L_b which they estimate to be ∼10 km. They also report that caprock thickness (a proxy for channel depth) increases downstream, consistent with backwater morphodynamics. The deposits studied by DiBiase et al. (2013) are visually separated from but genetically linked to those studied in this work (Cardenas & Lamb, 2022; Hughes et al., 2019).

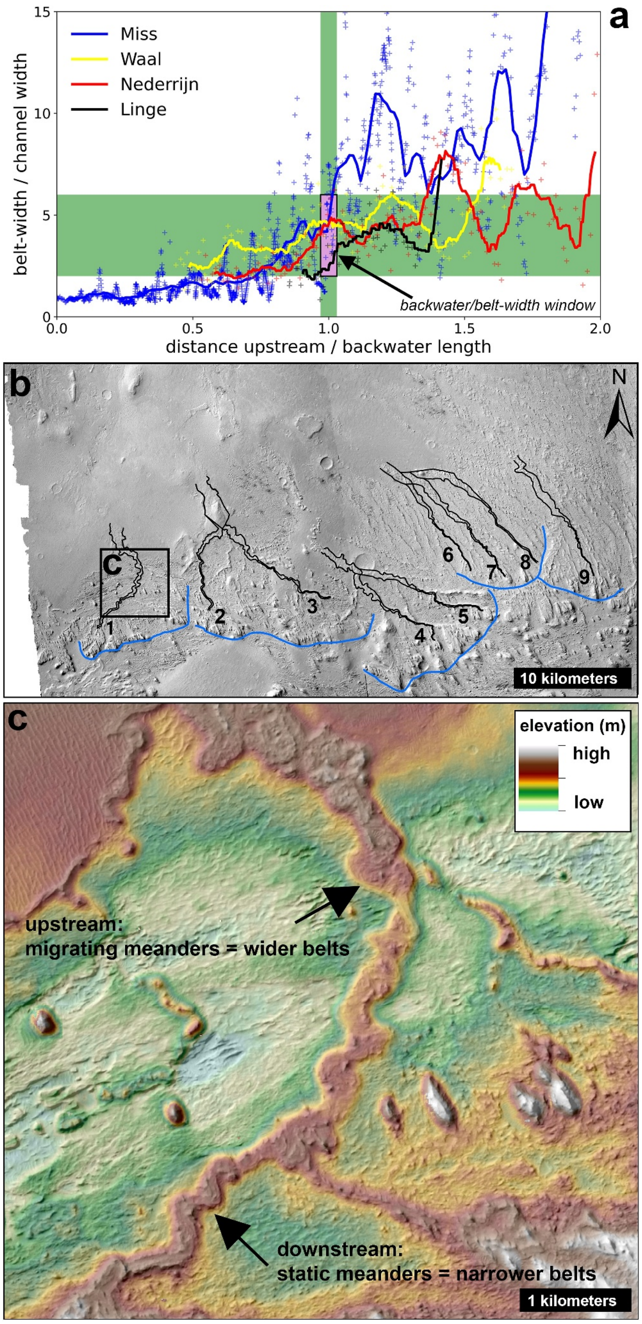

Figure 1. (a) CB width divided by a characteristic channel width (i.e., normalized CB width) plotted against normalized L_b for terrestrial CBs. Data is from Fernandes et al. (2016). Curves represent boxcar moving averages with a width of 0.1 L_b. The pink box indicates the *backwater/belt-width window*, roughly one L_b upstream (0.97–1.03), where channel-normalized widths fall between 2 and 6. (b) CTX mosaic of southeast Aeolis Dorsa, Mars, with CBs numbered. Lateral bounds outlined (black) and shorelines mapped (blue). (c) CTX orthoimages and DEMs show a type-example of a topographically inverted CB.

Here, we test the hypothesis that deltaic CBs on Mars narrow in association with backwater morphodynamics as they do on Earth. We present measurements of CBs in southeast Aeolis Dorsa which are used to determine the location of the *backwater/belt-width window*. From the *backwater/belt-width window*, we estimate L_b, depositional slope, and grainsize for each CB. The results of this study establish that backwater morphodynamics are a planetary phenomenon. They illustrate the scale of these deltas and provide novel mechanisms for further characterization martian fluvial systems and Mars' hydrologic and climatic history more broadly. This work adds veracity to observations from planet Earth (Fernandes et al., 2016; Martin et al., 2018; Wahbi & Blum, 2023; Wu et al., 2023). Lastly, the presence of backwater morphodynamics at Aeolis Dorsa provides independent evidence that the numerous fan-shaped deposits in this region are deltaic in origin and consistent with a northern hemispheric ocean (but cf. Burr, 2024).

2. Methods

2.1. Data

To visualize how channel-normalized width changes with distance upstream of the coastline in the terrestrial data set (Fernandes et al., 2016), and to highlight the extent of the backwater/belt-width window, we plotted measurements and moving averages using a box width of 0.1 L_b (Figure 1a). The backwater/belt-width window is defined statistically. It is centered on the mean normalized width, calculated from all data points located between 0.97 and 1.03 L_b upstream of the coastline. The vertical extent of the window spans one standard deviation above and below this mean. Channel-normalized widths at approximately one L_b upstream, rounded to the nearest integer, fall within a range of 2–6 (pink box, Figure 1a).

We mapped nine CBs from southeast Aeolis Dorsa using ESRI's ArcMap software (Figure 1b). Measurements were made using mosaicked stereo-photometry-derived digital elevation models (DEMs) and ortho-images from the Context Camera (CTX) aboard NASA's Mars Reconnaissance Orbiter. CTX takes panchromatic images with 6 m/pixel (Malin, 2007; Malin et al., 2007). DEMs are products of the NASA Ames Stereo Pipeline (ASP) (Beyer et al., 2018; Shean et al., 2016) through which they were also tied to Mars Orbiter Laser Altimeter data to minimize error associated with regional tilt (Beyer et al., 2018). CTX DEMs are 18 m/pixel with a vertical error of ~6 m/pixel. The CTX images pairs used are: B19_016981_1746-B21_017759_1746, B20_01758_1739-G02_019104_1740, and B17_016203_1744-B22_018260_1744.

2.2. Mapping

Given the abundance of ridges in the study area, we limited our analysis to those that were well-preserved and exhibited sufficient lateral continuity for reliable mapping. Heavily eroded areas were excluded. We specifically focused on ridges that narrowed in the downstream direction. In contrast, a singular deposit located immediately east of the study area was excluded due to its distinct character: it lacks the dendritic organization and ribbon-like narrowing of the nine measured channel belts. This deposit comprises an amalgamation of multiple deltaic lobes and exhibits complex stratigraphy (Hughes et al., 2019; their Figures 4 and 5), precluding its inclusion in this study.

10.1029/2024GL112957

It is worth noting that prior analog studies describe stacked channel bodies within single fluvial ridges (e.g., Cardenas et al., 2020; Hayden et al., 2019; Williams et al., 2009), which has been cited as a potential source of error in estimating channel and hydrologic parameters like those measured here. However, those analogs represent fluvial megafans, which are non-coastal systems and thus not subject to backwater effects. In contrast, recent work on a topographically inverted, Mississippian-aged delta in Northwest Arkansas shows that ridges in deltaic settings more commonly preserve single channel bodies (Hughes et al., 2024). This interpretation is consistent with well-established models of delta stratigraphy (e.g., Olariu & Bhattacharya, 2006).

Lateral CB boundaries were defined by a confining slope break (black polylines in Figure 1b). The downstream extent was defined by a lobate-style sand body or mound interpreted as a mouth bar deposit, marking the fluvial-marine transition. Shorelines were estimated based on erosional front of a given deposit (blue polylines in Figure 1b). The mapped deltas and estimated shorelines should be interpreted as a final snapshot of an otherwise dynamic system. Distance upstream was calculated from the shoreline along each CB centerline.

The width of a given CB was measured between lateral bounds, with spacing of ~100 m, perpendicular to the centerline. Widths were normalized using a characteristic channel width, determined by averaging one-third of the width measurements closest to the coastline. This method reflects the nature of distal channels in river delta systems which migrate minimally (e.g., Thomas et al., 2020; Wu et al., 2023). There is general uncertainty associated with the width measurements given that erosion has narrowed ridges since excavation, so all width values should be seen as lower bounds. To mitigate the effect of width uncertainty, measurements were performed in a consistent manner throughout the study area so erosional biases should affect all areas similarly. Crucially, assuming consistent ridge lithology and erosion throughout the area, the signal of systematic narrowing toward the coastline through the *backwater/belt-width window* should remain intact despite these uncertainties. Lastly, the visible scroll bar deposits visible in ridge tops indicate that less than one channel width of erosion has occurred in the sandy deposits (Figure 1c), indicating that the magnitude of ridge erosion may not substantively change the results of our measurements.

2.3. Analysis

By comparing normalized width to distance upstream, we were able to estimate L_b by applying the *backwater/belt-width window* for each CB (Figure 2). The range of distances that fall within the *window* provides estimates for L_b. As a standard of comparison, we mapped the location of lobe-scale avulsion nodes, defined by splits in the CB outcrop in the downstream direction. We noted when an avulsion node landed within the *backwater/belt-width window* and when outside (stars and circles respectively in Figure 3a). We also compared the distance upstream of each avulsion node to the median value of the corresponding *backwater/belt-width window(s)* (visualized in Figure 3a histogram). Furcations nearest to the coast were excluded from the avulsion node analysis; they are interpreted as mouth bar driven bifurcations rather than lobe-scale avulsions (Edmonds et al., 2009).

Channel depth estimates follow methods from DiBiase et al. (2013). Width-to-depth ratios range from 10 to 60 for single-thread rivers (Parker et al., 2007). Notably, systematic changes in channel depth in the backwater zone are well supported by previous studies (e.g., Nittrouer et al., 2012). However, the values from Parker et al. (2007) are consistent with measurements of the Mississippi River within the backwater zone (Nittrouer et al., 2012). We used 10 and 60 in our calculations to set upper and lower bounds for depth, multiplying each by CB characteristic width. Additional comparisons to the empirical results from Bridge and Mackey (1992) support these depth estimates. Once backwater length scale (L_b) and channel depth (h) were determined, we rearranged Equation 1 to solve for the slope (s). Dade and Friend (1998) demonstrate that slope is correlated with the median grainsize of the bed material normalized by channel depth. Based on these empirical relationships, we estimate grainsize. Our slope estimates bound d/h (after Figure 5 from Dade & Friend, 1998) to a maximum of 10^{-3} and a minimum of 10^{-5}.

3. Results

Measured CB widths range from 16 to 1,395 m for all belts (Table 1). Characteristic channel widths range from 36 to 155 m. We estimate L_b for nine different CBs in the southeast Aeolis Dorsa region of Mars and map the *backwater/belt-width window* for each in Figure 3a (orange regions). L_b estimates range from ~5 to 17 km with an average of 9.2 km. We calculate a range of estimates for slope for each channel belt (Table 1), and estimates range

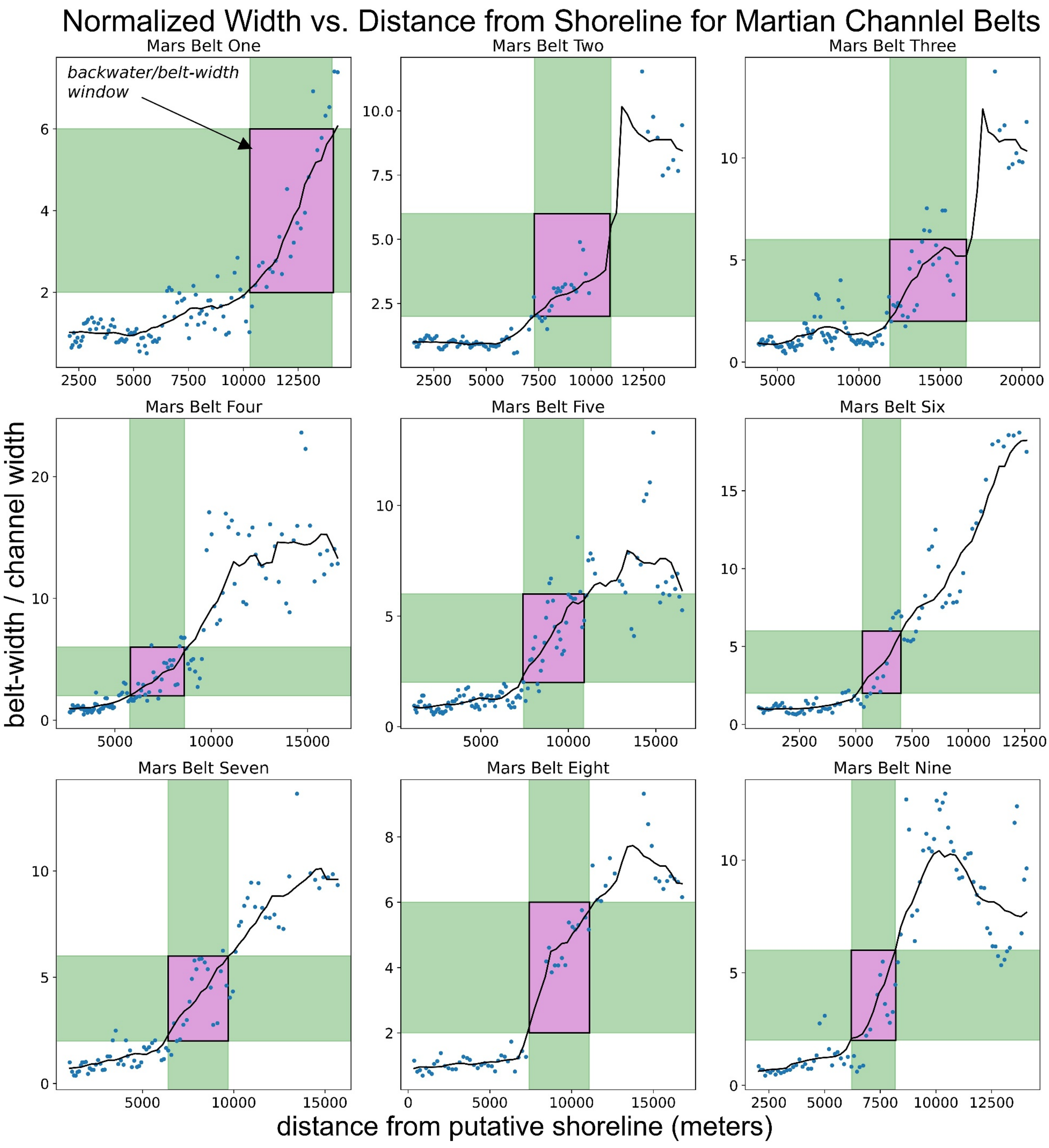

Figure 2. Channel-normalized width and distance from shoreline for the nine measured CBs in southeast Aeolis Dorsa. Curves represent moving averages with a box width of 5 km. Estimates for L_b are found using the *backwater/belt-width window*—when the average channel-normalized width crosses into the *backwater/belt-width window* (which is a range from 2 to 5 channel-normalized widths; pink rectangle) a range of distances from the putative shoreline can be found on the *x*-axis. These distances correspond to an estimate range for the length of the backwater zone for a given CB.

from ~5.5×10^{-5} to 1.9×10^{-3} with an average of 6.0×10^{-4}. Using the estimates of flow depth and slope we extrapolate grainsize estimates based on empirical relationships from terrestrial rivers (Dade & Friend, 1998). Median grainsizes of the bed material for these deposits range from 0.006 to 15.5 mm (silt to medium gravel). We identify eleven lobe-scale avulsion nodes that are located between 0.8 and 1.2 L_b (histogram and gold stars in Figure 3a). We also note that another eleven lobe-scale avulsion nodes are within a factor of two distance from each *backwater/belt-width window* and that all are within a factor of three.

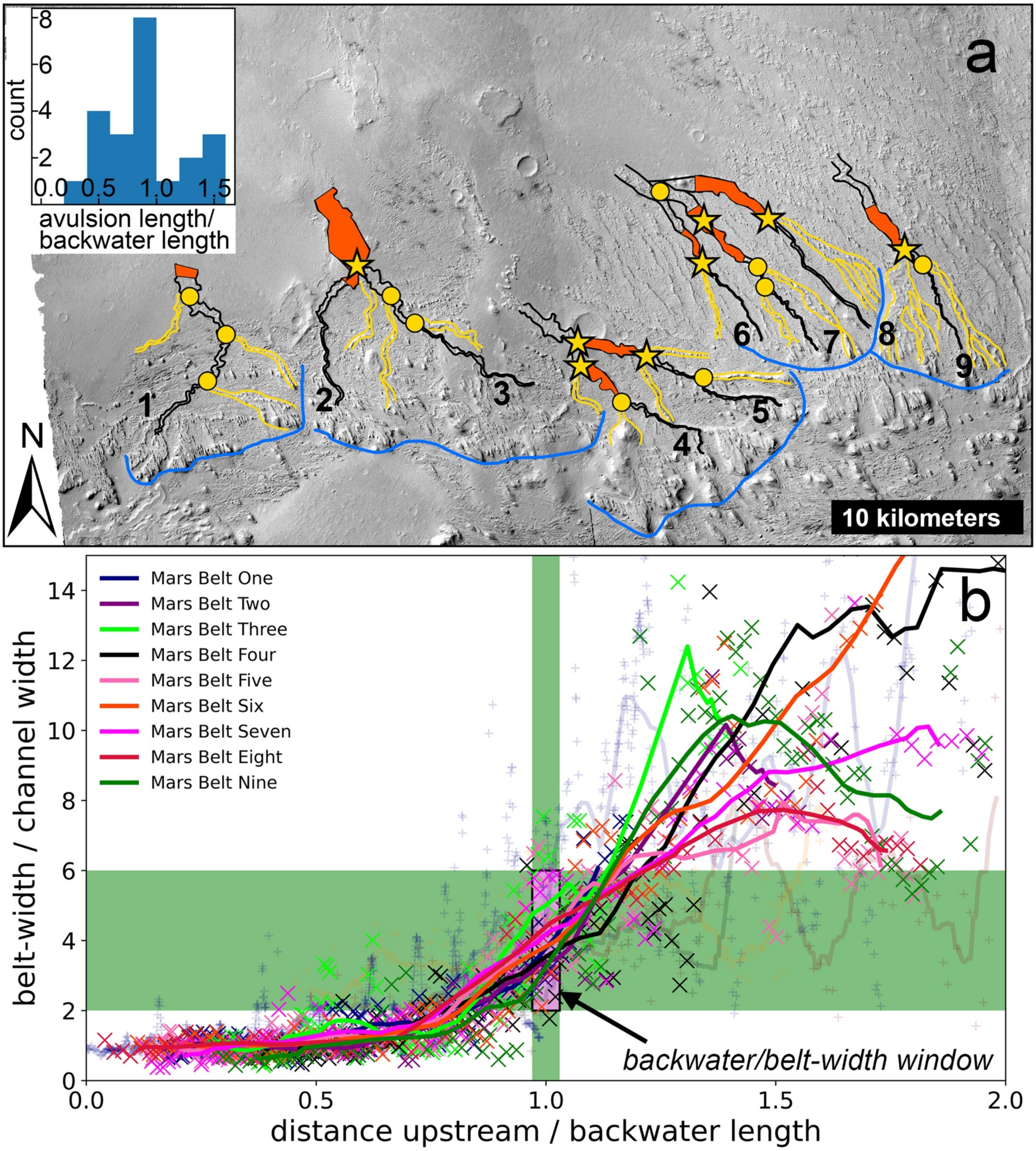

Figure 3. (a) Mapped CBs outlined in black and the putative shorelines in blue. Yellow outlines indicate avulsed CB paths. The *backwater/belt-width window* for each CB is shown in orange. Avulsion nodes are marked with gold stars and circles; stars when they fall within the *backwater/belt-width window*, and circles when they fall outside. Histogram shows the avulsion length of identified nodes (stars and circles) in terms of their distance upstream measured in backwater lengths. Note that most nodes are ~1 backwater length upstream. (b) Channel-normalized widths versus normalized backwater length for the martian CBs plotted on top of the Earth data (semi-transparent) from Fernandes et al. (2016).

4. Discussion

The most salient results from this study are (a) the confirmation of backwater morphodynamics in the stratigraphy in the northern hemisphere of Mars, and (b) the ensuing estimates for fluvial parameters (Table 1). The demonstration of narrowing channel belts confirms that backwater morphodynamics is a planetary phenomenon and can be expected to play a role in fluvial systems on all planetary bodies that host them (e.g., Earth, Mars, Titan). As we show, backwater morphodynamics can provide a unique suite of tools for characterizing and

Table 1
Estimated Parameters for Each Martian CB

Channel belt	Minimum width (meters)	Maximum width (meters)	Characteristic width (meters)	L_b (kilometers)	h (meters)	s	Grainsize (mm)
One	79	1,147	155	10.3–14.1	2.6–15.5	0.00016–0.00132	0.026–15.5
Two	68	1,395	121	7.3–10.9	2.0–12.1	0.00014–0.00141	0.02–12.1
Three	42	1,395	98	11.9–16.6	1.6–9.8	0.00009–0.00072	0.016–9.8
Four	17	850	36	5.8–8.6	0.6–3.6	0.00005–0.00053	0.006–3.6
Five	41	997	75	7.4–10.9	1.3–7.5	0.00009–0.00086	0.013–7.5
Six	26	768	41	5.3–7.0	0.7–4.1	0.00009–0.00068	0.007–4.1
Seven	29	1,063	78	6.4–9.7	1.3–7.8	0.0001–0.00102	0.013–7.8
Eight	79	1,053	113	7.4–11.1	1.9–11.3	0.00013–0.0013	0.019–11.3
Nine	25	764	134	6.2–8.2	2.2–13.4	0.00025–0.00192	0.022–13.4
Average	45	1,048	95	9.2	5.5	0.0006	4.7

Note. Mars CBs are numbered from west to east in Figures 1b and 3a. Calculated averages for estimations expressed as ranges (columns 3–6) reflect the average of the midpoints for each range.

parameterizing ancient fluvial systems, even with data sets that are collected from orbit. Estimates for such parameters on Mars are difficult to constrain given the remote nature of the outcrops. Estimating the depositional slope of martian fluvial systems is difficult, and direct measurements can be fraught with error. Similarly, grainsize is a particularly elusive parameter for martian fluvial systems (e.g., Dietrich et al., 2017; Presley & Craddock, 2006). Rover-based grainsize data is a notable exception; however, it is inherently limited geographically. New methods for estimating the median grainsize of bed material and slope are useful because they are crucial parameters for sedimentologic understanding of fluvial systems (e.g., Dietrich et al., 2017; Engelund & Hansen, 1967; Trampush et al., 2014), and they are essential for estimating the formation timescale of similar systems (e.g., Lapôtre & Ielpi, 2020).

4.1. Parameterization of Fluvial Systems

Our estimates for median grainsize (0.006–15.5 mm; silt to medium gravel) and slope ($\sim 5.5 \times 10^{-5}$ to 1.9×10^{-3}) agree with mature deltas on Earth (e.g., Syvitski & Saito, 2007), though gravel sized clasts are uncommon on Earth. However, recent work on the influence of reduced gravity indicates that martian rivers would move larger grains for equivalent discharge (Braat et al., 2024), and numerical modeling of martian fluvial systems indicates that gentler slopes may be expected in suspended load dominated regimes (Amy & Dorrell, 2021). The similarity between our estimates and terrestrial systems is consistent with theory comparing fluvial systems across planetary bodies (e.g., Birch et al., 2023). Notably, due to erosion and particularly for martian CBs four through seven, we suspect systematic underestimation of characteristic channel width. This results in dependent estimates of backwater length scale, grainsize, and depth also carrying some degree systematic underestimation with slope being similarly overestimated. Though, given the conservative ranges represented in our estimates (which are orders of magnitude larger than any systematic error), we consider these systematic errors to lack significant influence on our broader interpretations.

4.2. Climatic and Geographic Interpretations

Our results provide independent evidence of a standing body of water in the southeast Aeolis Dorsa region, which is consistent with an ancient northern hemispheric ocean. The colocation of the start of each backwater zone and the preserved avulsion nodes (stars and circles in Figure 3a) is consistent with theory linking backwater to avulsion location and with observations of long-lived, lowland river deltas on Earth, and (e.g., Brooke et al., 2022; Chatanantavet et al., 2012). Furthermore, based on flume experiments (Ganti et al., 2016) and empirical observation of terrestrial deltas (Brooke et al., 2020, 2022; Chadwick et al., 2019) the fact that avulsions on these martian deltas were backwater-modulated points to a non-trivial influence from flood events on the morphologic evolution of these systems. The co-location of the start of the backwater zone and the scale of the avulsions may also indicate that these martian river systems were not particularly fine-grained, did not have unusually high sediment loads, and their characteristic flood duration was shorter than the bed-adjustment timescale (Brooke et al., 2020).

The L_b estimates recorded in Table 1 reveal a sense of scale for these systems and provide a standard for comparison to other studies of similar outcrops in Aeolis Dorsa. Cardenas et al. (2018) and Ahmed et al. (2023) both studied deposits upstream from our study area. Cardenas et al. (2018) point to a backwater control on the stratigraphy, and while the rocks they study are further upstream than our estimates for backwater length (i.e., ~40 km), prior studies indicate the influence of base-level fluctuations can be recognized in stratigraphy substantially further upstream than the backwater zone (e.g., Shen et al., 2012; Wu & Nitterour, 2020). Ahmed et al. (2023) present estimates for backwater length (1.69–6.56 km) which overlap on the lower end of our estimates. Our range of estimates for backwater length is consistent with estimates from deposits to the northeast in Aeolis Dorsa studied by DiBiase et al. (2013) and which have also been linked to the deposits from this study (Cardenas & Lamb, 2022; Hughes et al., 2019).

Not all rivers produce CBs that narrow near the coastline. For example, rivers that enter the coastal region close to their headwaters (e.g., Haast river in New Zealand) and rivers with significant tidal influence show a relative increase in channel width in the downstream direction (e.g., Gugliotta & Saito, 2019). Swartz et al. (2020) also show that the Lower Rio Grande (Texas and Mexico) does not respond to backwater forcings in a manner consistent with theory and empirical studies (e.g., Fernandes et al., 2016). Their proposed mechanism for this deviation is a channel which remains adjusted solely for peak flow conditions, and which never adjusts to baseflow. Given the martian deposits analyzed here do not widen and agree with other backwater-modulated rivers, we can reasonably assume these rivers in southeast Aeolis Dorsa were not near their headwaters, experienced minimal tidal influence, and routinely readjusted between baselevel flow and peak flow stages.

5. Conclusions

Our results show that backwater morphodynamics are preserved in martian stratigraphy, confirming that this phenomenon is not unique to Earth. Measured channel belt narrowing in the Aeolis Dorsa region is consistent with Earth analogs and provides estimates for backwater length scales (5–17 km), slope, depth, and grainsize—parameters rarely accessible from orbit. The co-location of avulsion nodes and backwater zones further points to a dynamic, long-lived, lowland delta system influenced by flood variability. These observations offer independent evidence for a significant standing body of water in Mars' northern hemisphere and reinforce the interpretation of the fan-shaped deposits as river deltas. More broadly, this study demonstrates how empirical relationships from Earth can unlock the hydrologic history of other planets, offering a blueprint for reconstructing ancient landscapes across the solar system.

Data Availability Statement

CTX EDR data are available from the Planetary Data System (Malin, 2007). Shapefiles, data sets, and scripts are available in the Harvard Dataverse (Hughes, 2024).

Acknowledgments
This work was funded in part by a DOE grant awarded to JBS (DESC0016163). CMH received funding from the University of Arkansas. We thank Kevin Lewis and two anonymous reviewers for comments that improved the manuscript.

References

Ahmed, J., Peakall, J., Balme, M. R., & Parsons, D. R. (2023). Rapid megaflood-triggered base-level rise on Mars. *Geology*, *51*(1), 28–32. https://doi.org/10.1130/G50277.1

Amy, L., & Dorrell, R. (2021). Equilibrium sediment transport, grade and discharge for suspended-load-dominated flows on Earth, Mars and Titan. *Icarus*, *360*, 114243. https://doi.org/10.1016/j.icarus.2020.114243

Beyer, R. A., Alexandrov, O., & McMichael, S. (2018). The Ames stereo pipeline: NASA's open source software for deriving and processing terrain data. *Earth and Space Science*, *5*(9), 537–548. https://doi.org/10.1029/2018ea000409

Birch, S. P., Parker, G., Corlies, P., Soderblom, J. M., Miller, J. W., Palermo, R. V., et al. (2023). Reconstructing river flows remotely on Earth, Titan, and Mars. *Proceedings of the National Academy of Sciences of the United States of America*, *120*(29), e2206837120. https://doi.org/10.1073/pnas.2206837120

Braat, L., Brückner, M. Z., Sefton-Nash, E., & Lamb, M. P. (2024). Gravity-driven differences in fluvial sediment transport on Mars and Earth. *Journal of Geophysical Research: Planets*, *129*(2), e2023JE007788. https://doi.org/10.1029/2023JE007788

Bridge, J. S., & Mackey, S. D. (1992). A theoretical study of fluvial sandstone body dimensions. In *The geological modelling of hydrocarbon reservoirs and outcrop analogues* (pp. 213–236). https://doi.org/10.1002/9781444303957.ch14

Brooke, S. A. S., Chadwick, A. J., Silvestre, J., Lamb, M. P., Edmonds, D. A., & Ganti, V. (2022). Where rivers jump course. *Science*, *376*(6596), 987–990. https://doi.org/10.1126/science.abm1215

Brooke, S. A. S., Ganti, V., Chadwick, A. J., & Lamb, M. P. (2020). Flood variability determines the location of lobe-scale avulsions on deltas: Madagascar. *Geophysical Research Letters*, *47*(20), e2020GL088797. https://doi.org/10.1029/2020GL088797

Burr, D. M. (2024). An Aeolis Dorsa, Mars, formation scenario constrained by data other than sinuous ridge morphologies. In *10th Internation Conference on Mars: Geology, Geochemistry, and Mineralogy VII: Rivers, Lakes, and Oceans, Abstract No: 3018*.

Cardenas, B. T., & Lamb, M. P. (2022). Paleogeographic reconstructions of an ocean margin on Mars based on deltaic sedimentology at Aeolis Dorsa. *Journal of Geophysical Research: Planets*, *127*(10), e2022JE007390. https://doi.org/10.1029/2022JE007390

Cardenas, B. T., Mohrig, D., & Goudge, T. A. (2018). Fluvial stratigraphy of valley fills at Aeolis Dorsa, Mars: Evidence for base-level fluctuations controlled by a downstream water body. *GSA Bulletin*, *130*(3–4), 484–498. https://doi.org/10.1130/B31567.1

Cardenas, B. T., Mohrig, D., Goudge, T. A., Hughes, C. M., Levy, J. S., Swanson, T., et al. (2020). The anatomy of exhumed river-channel belts: Bedform to belt-scale river kinematics of the Ruby Ranch Member, Cretaceous Cedar Mountain Formation, Utah, USA. *Sedimentology*, *67*(7), 3655–3682. https://doi.org/10.1111/sed.12765

Chadwick, A. J., Lamb, M. P., Moodie, A. J., Parker, G., & Nittrouer, J. A. (2019). Origin of a preferential avulsion node on lowland river deltas. *Geophysical Research Letters*, *46*(8), 4267–4277. https://doi.org/10.1029/2019GL082491

Chatanantavet, P., Lamb, M. P., & Nittrouer, J. A. (2012). Backwater controls of avulsion location on deltas. *Geophysical Research Letters*, *39*(1). https://doi.org/10.1029/2011GL050197

Dade, W. B., & Friend, P. F. (1998). Grain-size, sediment-transport regime, and channel slope in alluvial rivers. *The Journal of Geology*, *106*(6), 661–676. https://doi.org/10.1086/516052

DiBiase, R. A., Limaye, A. B., Scheingross, J. S., Fischer, W. W., & Lamb, M. P. (2013). Deltaic deposits at Aeolis Dorsa: Sedimentary evidence for a standing body of water on the northern plains of Mars. *Journal of Geophysical Research: Planets*, *118*(6), 1285–1302. https://doi.org/10.1002/jgre.20100

Dietrich, W. E., Palucis, M. C., Williams, R. M., Lewis, K. W., Rivera-Hernandez, F., & Sumner, D. Y. (2017). Fluvial gravels on Mars: Analysis and implications. *Gravel-Bed Rivers: Processes and Disasters*, 755–783. https://doi.org/10.1002/9781118971437.ch28

Edmonds, D. A., Hoyal, D. C., Sheets, B. A., & Slingerland, R. L. (2009). Predicting delta avulsions: Implications for coastal wetland restoration. *Geology*, *37*(8), 759–762. https://doi.org/10.1130/G25743A.1

Engelund, F., & Hansen, E. (1967). *A monograph on sediment transport in alluvial streams* (Vol. 10). Technical University of Denmark Øster Voldgade.

Fawdon, P., Gupta, S., Davis, J. M., Warner, N. H., Adler, J. B., Balme, M. R., et al. (2018). The Hypanis Valles delta: The last highstand of a sea on early Mars? *Earth and Planetary Science Letters*, *500*, 225–241. https://doi.org/10.1016/j.epsl.2018.07.040

Fernandes, A. M., Törnqvist, T. E., Straub, K. M., & Mohrig, D. (2016). Connecting the backwater hydraulics of coastal rivers to fluvio-deltaic sedimentology and stratigraphy. *Geology*, *44*(12), 979–982. https://doi.org/10.1130/G37965.1

Ganti, V., Chadwick, A. J., Hassenruck-Gudipati, H. J., Fuller, B. M., & Lamb, M. P. (2016). Experimental river delta size set by multiple floods and backwater hydrodynamics. *Science Advances*, *2*(5). https://doi.org/10.1126/sciadv.1501768

Gibling, M. R. (2006). Width and thickness of fluvial channel bodies and valley fills in the geological record: A literature compilation and classification. *Journal of Sedimentary Research*, *76*(5), 731–770. https://doi.org/10.2110/jsr.2006.060

Goudge, T. A., Mohrig, D., Cardenas, B. T., Hughes, C. M., & Fassett, C. I. (2018). Stratigraphy and paleohydrology of delta channel deposits, Jezero crater, Mars. *Icarus*, *301*, 58–75. https://doi.org/10.1016/j.icarus.2017.09.034

Gugliotta, M., & Saito, Y. (2019). Matching trends in channel width, sinuosity, and depth along the fluvial to marine transition zone of tide-dominated river deltas: The need for a revision of depositional and hydraulic models. *Earth-Science Reviews*, *191*, 93–113. https://doi.org/10.1016/j.earscirev.2019.02.002

Hayden, A. T., Lamb, M. P., Fischer, W. W., Ewing, R. C., McElroy, B. J., & Williams, R. M. (2019). Formation of sinuous ridges by inversion of river-channel belts in Utah, USA, with implications for Mars. *Icarus*, *332*, 92–110. https://doi.org/10.1016/j.icarus.2019.04.019

Hudson, P. F., & Kesel, R. H. (2000). Channel migration and meander-bend curvature in the lower Mississippi River prior to major human modification. *Geology*, *28*(6), 531–534. https://doi.org/10.1130/0091-7613(2000)28<531:CMAMCI>2.0.CO;2

Hughes, C. M. (2024). Shapefiles and scripts for channel belt width measurements: Aeolis Dorsa, Mars. [Collection] Harvard Dataverse, V2, UNF:6:8MH/9sF0IOg/oZ+9e5qqNA== [fileUNF]. https://doi.org/10.7910/DVN/K6KVV5

Hughes, C. M., Cardenas, B. T., Goudge, T. A., & Mohrig, D. (2019). Deltaic deposits indicative of a paleo-coastline at Aeolis Dorsa, Mars. *Icarus*, *317*, 442–453. https://doi.org/10.1016/j.icarus.2018.08.009

Hughes, C. M., Shaw, J. B., & Cardenas, B. T. (2024). Sedimentology of a topographically inverted river delta in Northwest Arkansas: An important analog for Jezero Crater and other Martian deposits. In *10th Internation Conference on Mars: Geology, Geochemistry, and Mineralogy VII: Rivers, Lakes, and Oceans, Abstract No: 3452*.

Jerolmack, D. J., & Swenson, J. B. (2007). Scaling relationships and evolution of distributary networks on wave-influenced deltas. *Geophysical Research Letters*, *34*(23). https://doi.org/10.1029/2007GL031823

Lamb, M. P., Nittrouer, J. A., Mohrig, D., & Shaw, J. (2012). Backwater and river plume controls on scour upstream of river mouths: Implications for fluvio-deltaic morphodynamics. *Journal of Geophysical Research*, *117*(F1). https://doi.org/10.1029/2011JF002079

Lapôtre, M. G., & Ielpi, A. (2020). The pace of fluvial meanders on Mars and implications for the western delta deposits of Jezero Crater. *AGU Advances*, *1*(2), e2019AV000141. https://doi.org/10.1029/2019AV000141

Lapôtre, M. G., Ielpi, A., Lamb, M. P., Williams, R. M., & Knoll, A. H. (2019). Model for the formation of single-thread rivers in barren landscapes and implications for pre-Silurian and Martian fluvial deposits. *Journal of Geophysical Research: Earth Surface*, *124*(12), 2757–2777. https://doi.org/10.1029/2019JF005156

Li, J., Liu, H., Meng, X., Duan, D., Lu, H., Zhang, J., et al. (2025). Ancient ocean coastal deposits imaged on Mars. *Proceedings of the National Academy of Sciences of the United States of America*, *122*(9), e2422213122. https://doi.org/10.1073/pnas.2422213122

Malin, M. C. (2007). MRO context camera experiment data record level 0 V1.0 [Dataset]. *NASA Planetary Data System*. https://doi.org/10.17189/1520266

Malin, M. C., Bell, J. F., III., Cantor, B. A., Caplinger, M. A., Calvin, W. M., Clancy, R. T., et al. (2007). Context camera investigation on board the Mars reconnaissance orbiter. *Journal of Geophysical Research*, *112*(E5). https://doi.org/10.1029/2006JE002808

Martin, J., Fernandes, A. M., Pickering, J., Howes, N., Mann, S., & McNeil, K. (2018). The stratigraphically preserved signature of persistent backwater dynamics in a large paleodelta system: The Mungaroo Formation, North West Shelf, Australia. *Journal of Sedimentary Research*, *88*(7), 850–872. https://doi.org/10.2110/jsr.2018.38

Nittrouer, J. A., Shaw, J., Lamb, M. P., & Mohrig, D. (2012). Spatial and temporal trends for water-flow velocity and bed-material sediment transport in the lower Mississippi River. *Bulletin*, *124*(3–4), 400–414.

Olariu, C., & Bhattacharya, J. P. (2006). Terminal distributary channels and delta front architecture of river-dominated delta systems. *Journal of Sedimentary Research*, *76*(2), 212–233. https://doi.org/10.2110/jsr.2006.026

Pain, C. F., Clarke, J. D. A., & Thomas, M. (2007). Inversion of relief on Mars. *Icarus*, *190*(2), 478–491. https://doi.org/10.1016/j.icarus.2007.03.017

Paola, C., & Mohrig, D. (1996). Palaeohydraulics revisited: Palaeoslope estimation in coarse-grained braided rivers. *Basin Research*, *8*(3), 243–254. https://doi.org/10.1046/j.1365-2117.1996.00253.x

Parker, G., Wilcock, P. R., Paola, C., Dietrich, W. E., & Pitlick, J. (2007). Physical basis for quasi-universal relations describing bankfull hydraulic geometry of single-thread gravel bed rivers. *Journal of Geophysical Research*, *112*(F4). https://doi.org/10.1029/2006JF000549

Presley, M. A., & Craddock, R. A. (2006). Thermal conductivity measurements of particulate materials: 3. Natural samples and mixtures of particle sizes. *Journal of Geophysical Research*, *111*(E9). https://doi.org/10.1029/2006JE002706

Shaw, J. B., & McElroy, B. (2016). Backwater number scaling of alluvial bed forms. *Journal of Geophysical Research: Earth Surface*, *121*(8), 1436–1455. https://doi.org/10.1002/2016JF003861

Shean, D. E., Alexandrov, O., Moratto, Z. M., Smith, B. E., Joughin, I. R., Porter, C., & Morin, P. (2016). An automated, open-source pipeline for mass production of digital elevation models (DEMs) from very-high-resolution commercial stereo satellite imagery. *ISPRS Journal of Photogrammetry and Remote Sensing*, *116*, 101–117. https://doi.org/10.1016/j.isprsjprs.2016.03.012

Shen, Z., Törnqvist, T. E., Autin, W. J., Mateo, Z. R. P., Straub, K. M., & Mauz, B. (2012). Rapid and widespread response of the Lower Mississippi River to eustatic forcing during the last glacial-interglacial cycle. *Bulletin*, *124*(5–6), 690–704. https://doi.org/10.1130/B30449.1

Smith, V., Mason, J., & Mohrig, D. (2020). Reach-scale changes in channel geometry and dynamics due to the coastal backwater effect: The lower Trinity River, Texas. *Earth Surface Processes and Landforms*, *45*(3), 565–573. https://doi.org/10.1002/esp.4754

Swartz, J. M., Goudge, T. A., & Mohrig, D. C. (2020). Quantifying coastal fluvial morphodynamics over the last 100 years on the lower Rio Grande, USA and Mexico. *Journal of Geophysical Research: Earth Surface*, *125*(6), e2019JF005443. https://doi.org/10.1029/2019JF005443

Syvitski, J. P., & Saito, Y. (2007). Morphodynamics of deltas under the influence of humans. *Global and Planetary Change*, *57*(3–4), 261–282. https://doi.org/10.1016/j.gloplacha.2006.12.001

Te Chow, V. (1959). Open channel hydraulics.

Thomas, J., Kumar, S., & Sudheer, K. P. (2020). Channel stability assessment in the lower reaches of the Krishna River (India) using multi-temporal satellite data during 1973–2015. *Remote Sensing Applications: Society and Environment*, *17*, 100274. https://doi.org/10.1016/j.rsase.2019.100274

Trampush, S. M., Huzurbazar, S., & McElroy, B. (2014). Empirical assessment of theory for bankfull characteristics of alluvial channels. *Water Resources Research*, *50*(12), 9211–9220. https://doi.org/10.1016/j.rsase.2019.100274

Wahbi, A. M., & Blum, M. D. (2023). Downstream morphological and sedimentary transformations in modern continental-scale rivers. *The Sedimentary Record*, *21*(1). https://doi.org/10.2110/001c.90009

Williams, R. M., Irwin, R. P., III., & Zimbelman, J. R. (2009). Evaluation of paleohydrologic models for terrestrial inverted channels: Implications for application to Martian sinuous ridges. *Geomorphology*, *107*(3–4), 300–315. https://doi.org/10.1016/j.geomorph.2008.12.015

Wu, C., & Nitterour, J. A. (2020). Impacts of backwater hydrodynamics on fluvial–deltaic stratigraphy. *Basin Research*, *32*(3), 567–584. https://doi.org/10.1111/bre.12385

Wu, C., Nittrouer, J. A., Barefoot, E. A., & Burmeister, K. C. (2023). Reconstructing backwater hydrodynamics from fluvial-deltaic deposits using stratigraphic inversion: An example from the Tullig Sandstone, Western Irish Namurian Basin, County Clare, Ireland. *Bulletin*, *135*(9–10), 2315–2330. https://doi.org/10.1130/B36475.1